

UC Berkeley

UC Berkeley Previously Published Works

Title

Modified Schwarzschild metric from a unitary accelerating mirror analog

Permalink

<https://escholarship.org/uc/item/5180d0gv>

Journal

New Journal of Physics, 23(4)

ISSN

1367-2630

Authors

Good, Michael RR
Linder, Eric V

Publication Date

2021-04-01

DOI

10.1088/1367-2630/abe506

Peer reviewed

PAPER • OPEN ACCESS

Modified Schwarzschild metric from a unitary accelerating mirror analog

To cite this article: Michael R R Good and Eric V Linder 2021 *New J. Phys.* **23** 043007

View the [article online](#) for updates and enhancements.



PAPER

Modified Schwarzschild metric from a unitary accelerating mirror analog

OPEN ACCESS

RECEIVED

16 November 2020

REVISED

7 February 2021

ACCEPTED FOR PUBLICATION

10 February 2021

PUBLISHED

2 April 2021

Michael R R Good^{1,2,*} and Eric V Linder^{2,3}¹ Physics Department, Nazarbayev University, Nur-Sultan, Kazakhstan² Energetic Cosmos Laboratory, Nazarbayev University, Nur-Sultan, Kazakhstan³ Berkeley Center for Cosmological Physics & Berkeley Lab, University of California, Berkeley, CA, United States of America

* Author to whom any correspondence should be addressed.

E-mail: omniver@gmail.com**Keywords:** black holes, moving mirrors, dynamical Casimir effect, Hawking radiation

Original content from this work may be used under the terms of the [Creative Commons Attribution 4.0 licence](https://creativecommons.org/licenses/by/4.0/).

Any further distribution of this work must maintain attribution to the author(s) and the title of the work, journal citation and DOI.



Abstract

We present a modified Schwarzschild solution for a model of evaporation of a black hole with information preservation. By drawing a direct analogy to the quantum pure accelerating mirror (dynamical Casimir effect of a 1D horizon), we derive a Schwarzschild metric with not only the usual Schwarzschild radius but an additional length scale related to the Planck length. The black hole has thermal particle production that leads to complete evaporation of the black hole, resulting in non-divergent entanglement entropy, Page curve turn-over, and an asymptotic quantum pure state with no information loss.

1. Introduction

Particle production from black holes, or more generally curved spacetime, is a fascinating process, bringing together quantum physics and gravity (or its Equivalence Principle partners of acceleration or curvature). Particles can be produced through

- Expanding Cosmologies (Parker effect [1])
- Black Holes (Hawking effect [2])
- Uniform acceleration Radiation (Unruh effect [3])
- Moving mirrors (Davies–Fulling effect [4–6])

Beyond the mere existence of this interesting physical process, we might seek for two characteristics with long ties to the development of quantum theory: finite global particle count (e.g. avoidance of divergent numbers of soft photons [7]) and a thermal (blackbody) radiation spectrum. Furthermore, the information carried by the radiation, and whether it is preserved or lost, is the subject of intense scrutiny [8].

Here we look at the simplest black hole case, that of the Schwarzschild metric, and explore a model for its formation and evaporation with information preservation. We motivate that this leads to introduction of a second length scale beyond the horizon size (which suggestively can be related to the Planck length), and explore what happens near the horizon and asymptotically, as well as when the horizon size approaches the new ‘quantum’ length scale after long evaporation. We emphasize that we do not introduce a second length scale to the Schwarzschild metric ad hoc, but rather derive it by adopting the principle of quantum purity that keeps key particle radiation quantities finite and well behaved [19].

We approach the issue through the analog particle radiation from moving mirrors, which have proved themselves very useful in different contexts. These $(1 + 1)$ -dimensional analog models have a long history and extensive literature (see [11–13] for an introduction) since they are much simpler: acceleration is easier to deal with than the $(3 + 1)$ -dimensional strong gravity systems they imitate. They therefore may admit exact and relatively simple analytical solutions that nevertheless faithfully capture key quantities and often provide some insight into the real effects. While the full quantum effects of a Planck length modification of Schwarzschild spacetime is beyond the scope of this paper, the moving mirror model can point the way to interesting implications for thermal particle production associated with Schwarzschild spacetime.

In section 2 we introduce the model and compute the spacetime geometric quantities. We study the particle production in section 3 in various limits, including the spectrum, total energy, and entropy, and quantum pure states. Section 4 summarizes and concludes.

2. Schwarzschild and Planck

The Schwarzschild metric describes a static black hole spacetime, and is central to exploring the physics of black holes, one of the most challenging subjects in physics. It can be derived based on certain symmetry principles of the spacetime, and Einstein's equations for gravity. It is a key stage on which we explore extremes of gravitational physics, and its Frontier with quantum physics. A black hole produces particles [2] from the spacetime by quantum physics, but neither the metric nor Einstein's equations reflect quantum physics. The particles radiate [3, 4] to infinity in the external spacetime, yet the external state is taken to be vacuum. What happens when the black hole radiates all its energy is unknown, and the subject of information paradoxes [8, 9]. Here we attempt to explore methods [10, 11] for probing these inconsistencies and puzzles.

2.1. Schwarzschild

In the classical picture, the Schwarzschild metric can be written as

$$ds^2 = -f_s dt^2 + f_s^{-1} dr^2 + r^2 d\Omega, \quad (1)$$

where the angular part of the metric is spherically symmetric, $d\Omega \equiv d\theta^2 + \sin^2 \theta d\phi^2$, and

$$f_s = 1 - \frac{r_s}{r}, \quad (2)$$

where $r_s = 2M$ is the Schwarzschild radius (related to the black hole mass M).

For studying the structure of spacetime, it is convenient to follow null rays and remove the coordinate singularity at $r = r_s$. This can be done with the Regge–Wheeler tortoise coordinate

$$r^* = r + r_s \ln \left| \frac{\Delta}{r_s} \right|, \quad (3)$$

where $\Delta \equiv r - r_s$. Rays of constant $t \pm r^*$ correspond to ingoing and outgoing null geodesics, and we can define

$$v = t + r^* \quad u = t - r^*, \quad (4)$$

for outside coordinates, and the equivalent V and U for inside coordinates, $T \pm r$ to describe a dynamic collapse model of evaporation, as we shall see. The derivative of the transformation gives the metric,

$$\frac{dr^*}{dr} \equiv f_s^{-1}. \quad (5)$$

The canonical collapse prescription (see e.g. [11, 12]) for a shell of matter at v_0 , where the horizon $v_H = v_0 - 2r_s$, gives the matching condition utilizing the regularity condition effect on the form of the modes, $v \leftrightarrow U$ [11]

$$u(U) = U - 4M \ln \left| \frac{U}{4M} \right| = U - \frac{1}{\kappa} \ln |\kappa U|, \quad (6)$$

where $\kappa = 1/(4M) = 1/(2r_s)$ is the surface gravity of the black hole. Note that $du/dU = f_s^{-1}(u, v_0)$ which results from differentiation of the implicit gauge-invariant radial coordinate matching [12]. We are free to set $v_H = 0$ without loss of generality, see also [13]. The collapse of the null shell along the null ray v_0 models the evaporation of the Schwarzschild black hole in allowing a simple derivation of the thermal spectrum associated with the Hawking effect.

At this point, we can draw attention to the analogy of a black hole, and its quantum physical particle production, to the Davies–Fulling effect [5, 6] for particle production by an accelerating mirror. This basically arises due to boundary conditions imposed on the spacetime, a dynamical Casimir effect, in much the same way that the black hole horizon is a boundary. Crafting the mirror trajectory to match the null coordinate form $u(U)$ in equation (6), i.e. identifying this as the trajectory of the origin in null coordinates of the mirror [14],

$$f_b(v) = v - \frac{1}{\kappa} \ln |\kappa v|, \quad (7)$$

gives what is known as the black mirror [15–17] or simply, the Schwarzschild mirror, which has the same late-time eternal thermal particle production as a Schwarzschild black hole. In the light-cone coordinates, f_b

is the retarded time, $u = t - x$, position as a function of advanced time $v = t + x$. The subscript refers to the canonical black mirror model for the Schwarzschild mirror. The coordinate x is the usual single space dimension of $(1 + 1)$ flat Minkowski spacetime.

Let us review our path. From the metric derived from the symmetries of spacetime and gravity, we moved to tortoise coordinates, matching conditions for collapse, and an analogy to particle production from a moving mirror. In the next subsection we will reverse this journey in the hope of learning something fundamental about spacetime around black holes with quantum physics of unitarity included.

2.2. Planck

The problem with the black mirror is that the analogy is too perfect. The particle production at late times is in eternal equilibrium, giving rise to an infinite number of particles and infinite total energy, as well as a black hole that simply radiates forever. The information paradox is a concern here (for much of the community at least, e.g. harvesting entanglement via the black mirror [18]) because violation of unitarity may contradict basic principles of probability and quantum theory. This black mirror-black hole model does not sufficiently clarify the connection between quantum physics and gravity.

However, recently a different sort of moving mirror trajectory was discovered [19], the quantum pure black mirror. This has both finite number of particles produced and finite total energy, acts like a black hole that evaporates completely [20] without leaving a remnant, and produces quasi-thermal radiation that ends in a pure quantum state. Entropy [21–24] is well behaved and there is no information loss. We wish to extend the lessons learned about this mirror further into the curved spacetime context of the Schwarzschild black hole.

The trajectory, f_p , of the quantum pure black mirror is

$$f_p(v) = v - \frac{1}{\kappa} \sinh^{-1}|gv|, \quad (8)$$

where there is now a new parameter g in addition to κ . Basically κ will determine the amplitude of the particle flux produced (in the same way that in the black hole case the surface gravity or mass does), while g will factor into the evaporation of the black hole, i.e. the lifetime. Just as we write $\kappa = 1/(2r_s)$, we can write $g = 1/(2l)$ and anticipate that l will be related to the Planck length $l_p = \sqrt{\hbar G/c^3}$. This will allow quantum physics and gravity to both enter the picture, i.e. we assume quantum purity from the start and investigate the resulting changes to the gravitational system.

Now we reverse our journey of the last subsection. We take the collapse condition in the black hole case in exact analogy to equation (8), so

$$u(U) = U - 2r_s \sinh^{-1} \left| \frac{U}{2l} \right|, \quad (9)$$

and define from this a quantum tortoise coordinate

$$\bar{r}^* = r + r_s \sinh^{-1} \left| \frac{\Delta}{l} \right|. \quad (10)$$

Up to a constant⁴, the quantum tortoise coordinate, equation (10), goes to the classical tortoise coordinate, equation (3),

$$\lim_{\mathcal{R} \rightarrow 0} \bar{r}^* = r^*, \quad \text{for } r > r_s, \quad (11)$$

where $\mathcal{R} \equiv l/r_s$. See the next subsection for more discussion.

Using that $d\bar{r}^*/dr \equiv \bar{f}^{-1}$ we now have our quantum replacement for the outside ($v = t + \bar{r}^* > v_0$) Schwarzschild static metric (see equation (2.3) of Wilczek [12]):

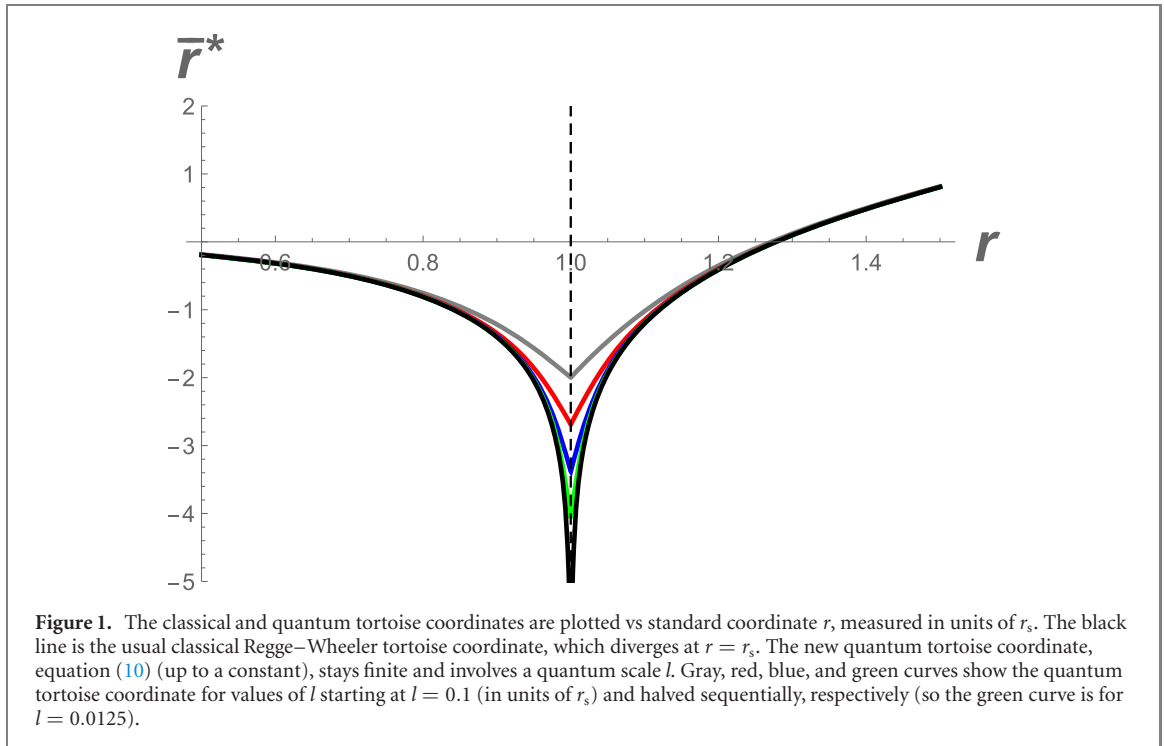
$$ds^2 = -\bar{f} dt^2 + \bar{f}^{-1} dr^2 + r^2 d\Omega, \quad (12)$$

where instead of the usual $f = 1 - r_s/r$, we have

$$\bar{f} \equiv 1 - \frac{r_s}{r_s + \sqrt{\Delta^2 + l^2}}, \quad (13)$$

with $\Delta \equiv r - r_s$. Clearly, when $l \rightarrow 0$, then $\bar{f} \rightarrow f$ gives the classical Schwarzschild solution. However, now there are further effects expected when $r - r_s \lesssim l$, e.g. within some Planck lengths of the horizon. And if l is indeed connected with the Planck length, then this is a quantum metric in the sense that $g_{\mu\nu}$ includes \hbar .

⁴ The constant can be found by setting $\bar{r}^* = r^* = 0$ and $r = 1 + W(1/e)$ in units of r_s . Here W is the Lambert W function.



To explore the effects of this new metric further, we investigate the Kretschmann scalar, which gives an invariant description of the curvature and singularities, the Ricci scalar, and the Einstein tensor. To leading order in l/r_s beyond the classical values (see appendix A for full expressions), near $r = r_s$, the scalars are,

$$K = \frac{12r_s^2}{r^6} - \frac{4l^2}{r_s^3\Delta^3} + \dots, \quad (14)$$

$$R = 0 - \frac{l^2}{r_s\Delta^3} + \dots \quad (15)$$

while the Einstein tensor is,

$$G_{\mu\nu} = 0 + \quad (16)$$

$$\begin{pmatrix} \frac{\Delta^2}{r_s^2} & & & \\ & -1 & & \\ & & r_s^2 & \\ & & & r_s^2 \sin^2 \theta \end{pmatrix} \frac{l^2}{2r_s\Delta^3} + \dots \quad (17)$$

Indeed when l vanishes we recover the classical Schwarzschild vacuum solution. However, there are several new aspects that arise with finite l . This is no longer a vacuum solution, i.e. $G_{\mu\nu} \neq 0$. That makes sense: for one thing the classical Schwarzschild metric is the unique vacuum solution for this spacetime, and for another we know there is particle production—we must break the vacuum solution. In a sense, since black holes radiate then the classical Schwarzschild metric should not be the true metric. We also see that when we are within some Planck lengths of the horizon, i.e. $\Delta = |r - r_s| \lesssim l$, that the Kretschmann and Ricci scalars deviate strongly from the classical behavior. We discuss this in detail in appendix A.

2.3. Classical and quantum, black hole and mirror

Our attempt to move from the classical to the quantum used the moving mirror analogy to suggest a new, quantum tortoise coordinate. Both the classical and quantum tortoise coordinates are plotted in figure 1. Note the quantum tortoise coordinate removes the divergence of the classical tortoise coordinate.

The moving mirror analog to a black hole is useful not only in describing particle flux, but spacetime structure, singularities, and asymptotic conditions as well. Figure 2 illustrates the classical correspondence in terms of a conformal spacetime diagram, with the mirror on the left and the black hole on the right. Note the strict v -horizon at v_H (black dotted line), which gives a divergent $f_b(v)$, signaling ‘incomplete’ evaporation—information loss.

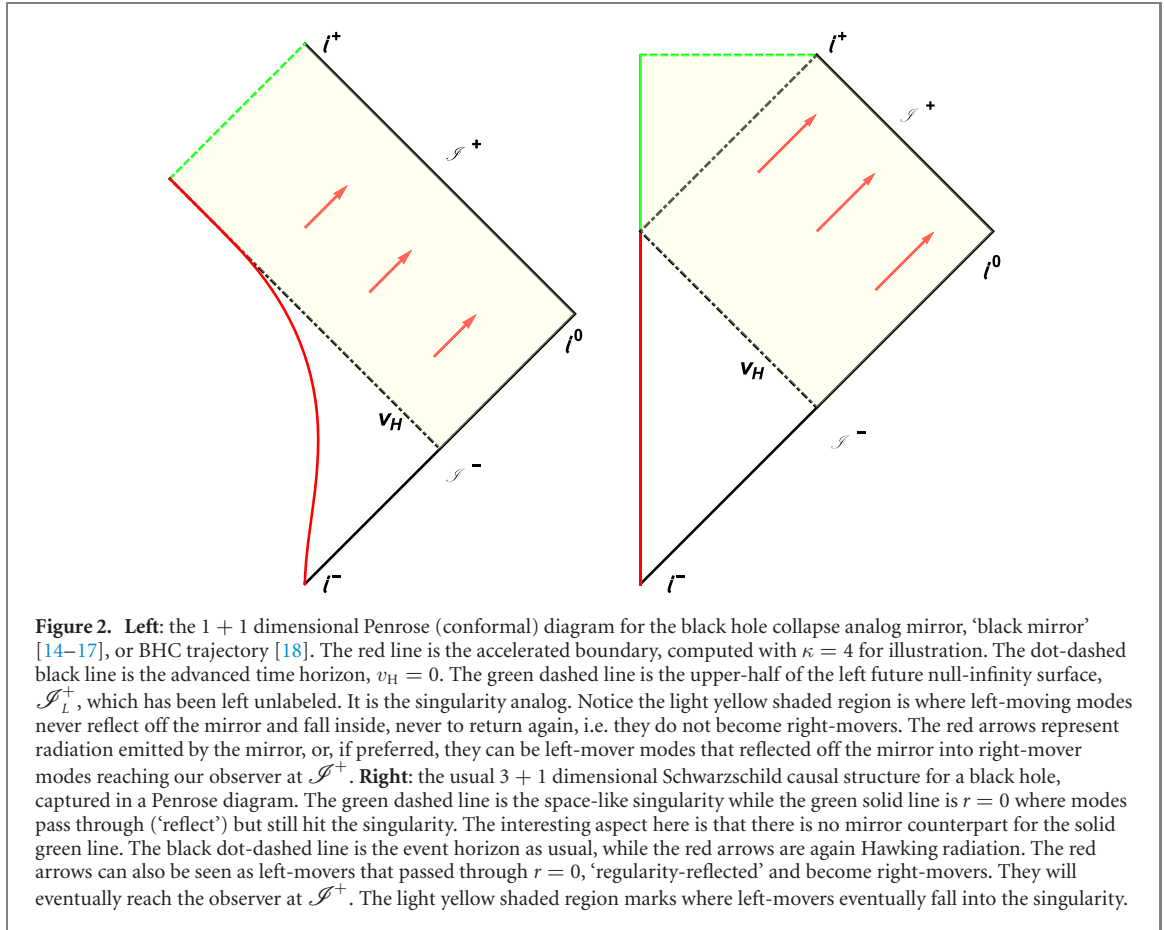


Figure 3 by contrast shows the new ‘quantum’ situation. The lack of a strict v -horizon in equation (8), contrasted with equation (7), signals complete evaporation—no information loss. Moreover, there is no remnant (see the contrasting cases where the modes are affected long after the radiation stops, e.g. [25–28]), since the field modes have the same early-time and late-time form (the mirror comes back to rest so there is no eternal redshift, e.g. [12, 20, 29]).

3. Particle production

The modes of the quantum field determine the particle production [30]. One of the powerful aspects of the quantum pure black mirror is the analytic expression for the Bogolyubov beta coefficients [19], allowing simple computation of the particle production properties (e.g. the spectrum [31]). The energy radiated also takes a simple expression (in the 1 + 1 dimensional context, at least). In the following subsections we discuss several of these properties.

3.1. Spatial and temporal limits

The field must be zero at the origin, as no field exists in $r < 0$. Regularity forces the form of the field modes

$$\phi_\omega^{\text{out}} = \frac{1}{4\pi r \sqrt{\omega}} (e^{-i\omega u(v)} - e^{-i\omega u(U)}), \quad (18)$$

where ω is the frequency, to assume

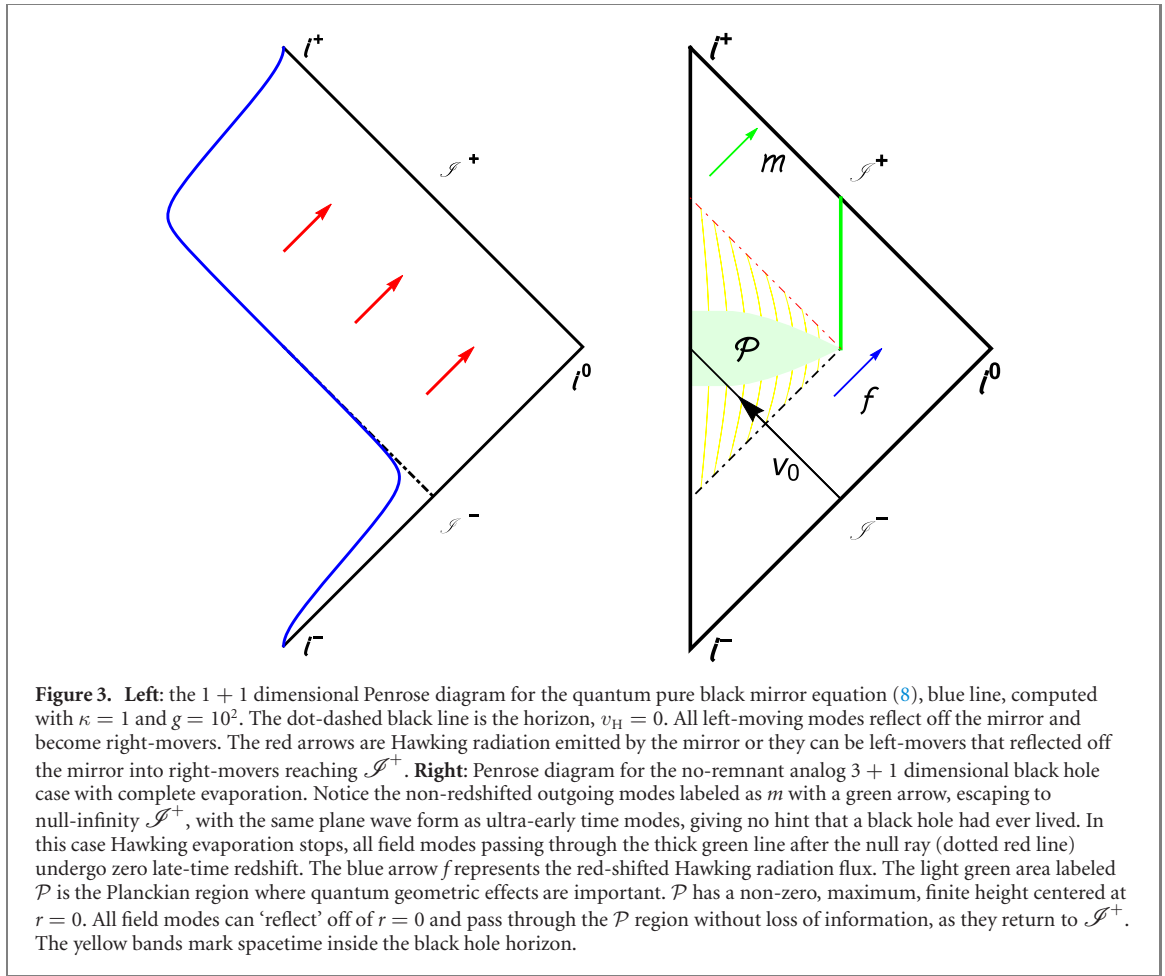
$$u(v) = u(U). \quad (19)$$

Therefore we write the matching condition equation (9), as

$$u(v) = v - 2r_s \sinh^{-1} \left| \frac{v}{2l} \right|. \quad (20)$$

This will be used in the modes to determine the behavior of the quantum field. A complete cover of the collapse spacetime is given in appendix B.

Armed with the matching condition, it is instructive to analyze the behavior of the modes at very early and at ultra-late times. We also look at a third temporal limit—the equilibrium times.



3.1.1. Early times

At early times, when $v \rightarrow -\infty$, we have $u(v) \approx v$. This is analogous to the mirror in the asymptotic past being at rest. When $U \rightarrow -\infty$, the matching condition equation (9) implies $u(U) \approx U$. Therefore at \mathcal{S}^- , early times,

$$\phi_\omega^{\text{out}} \approx \frac{1}{4\pi r \sqrt{\omega}} e^{-i\omega v}, \quad (21)$$

where the mode at $u \rightarrow -\infty$ is a pure positive frequency mode with respect to inertial time at \mathcal{S}^- . The Bogolyubov beta coefficients vanish and asymptotically early times exhibit no particle creation. There is nothing new here from the canonical case. There are no particles yet because the black hole has not formed, and its progenitor is only just beginning to collapse.

3.1.2. Equilibrium times

With the regularity condition, the exact mode form assumes

$$\phi_\omega^{\text{out}} = \frac{1}{4\pi r \sqrt{\omega}} \left(e^{-i\omega(v-2r_s \sinh^{-1}|\frac{v}{2l}|)} - e^{-i\omega u} \right), \quad (22)$$

and at \mathcal{S}^- where the u piece has infinite oscillation, the mode

$$\phi_\omega^{\text{out}} = \frac{1}{4\pi r \sqrt{\omega}} e^{-i\omega(v-2r_s \sinh^{-1}|\frac{v}{2l}|)}, \quad (23)$$

displays a strong blueshift in the exponent. Near the ‘horizon’ $v_H = 0$, the mode becomes

$$\phi_\omega^{\text{out}} = \frac{1}{4\pi r \sqrt{\omega}} e^{-i\omega(1+\frac{r_s}{l})v}, \quad (24)$$

typical of the process of black hole evaporation, which will largely modify the physics as calculated from the modes. Since $r_s \gg l$, it is particularly easy to see the geometric modification of the field. The form of the modes at intermediate times gives non-zero beta coefficients, resulting in particle creation. Moreover, the particular betas result in a quasi-thermal particle spectrum (see section 3.4).

3.1.3. Ultra-late times

At ultra-late times, when $v \rightarrow +\infty$, we have $u(v) \approx v$, again, like the situation at early times. This is seen because $U \rightarrow +\infty$, the matching condition equation (9), implies $u(U) \approx U$. Therefore at \mathcal{I}^- , ultra-late times,

$$\phi_\omega^{\text{out}} \approx \frac{1}{4\pi r \sqrt{\omega}} e^{-i\omega v}, \quad (25)$$

where the mode at $u \rightarrow +\infty$ is a pure positive frequency mode with respect to inertial time at \mathcal{I}^- . The beta coefficients vanish. At asymptotically ultra-late times there is no more particle creation, and one observes complete evaporation. Unitarity is maintained.

3.2. Radiation stress energy

Neglecting the time-independent Boulware vacuum polarization terms, specializing to conformal symmetry of 1 + 1 dimensions, the time-dependent non-zero component of the normal-ordered (denoted by colons) stress tensor in the in-vacuum state is computed as the Schwarzian derivative [11],

$$F(u) \equiv \langle \text{in} | : T_{uu}(u) : | \text{in} \rangle = -\frac{\hbar}{24\pi} \{U(u), u\}. \quad (26)$$

This is most easily done by utilizing the invariant,

$$\{u(U), U\} \left(\frac{du(U)}{dU} \right)^{-1} = \{U(u), u\} \left(\frac{dU(u)}{du} \right)^{-1}, \quad (27)$$

and substituting $u(U)$ from equation (9). As long as $r_s \gg l$, then to leading order the result is the usual canonical case [32]

$$F(u) = -\frac{\hbar}{24\pi} \left(\frac{2r_s(2U - r_s)}{(U - 2r_s)^4} \right). \quad (28)$$

Here $v_0 = 2r_s$. The analytic full-order solution is in appendix C, equation (C7). The thermal flux as the horizon is approached, $U \rightarrow 0$,

$$F_{\text{Hawking}} = \frac{\hbar}{192\pi r_s^2}, \quad (29)$$

suggests that equilibrium conditions expected of a long-lived (flux plateau, e.g. [33]) radiating black hole will demonstrate a consequent Planckian distribution of particle count for some limited period of time.

3.3. Evaporative energy

Conformal symmetry provides the additional benefit of calculable total energy in the limit $l \ll r_s$, such that [19]

$$E = \frac{\hbar c^3}{96\pi GM} \ln \frac{r_s}{l} = \frac{T_H}{12} \ln \frac{r_s}{l}. \quad (30)$$

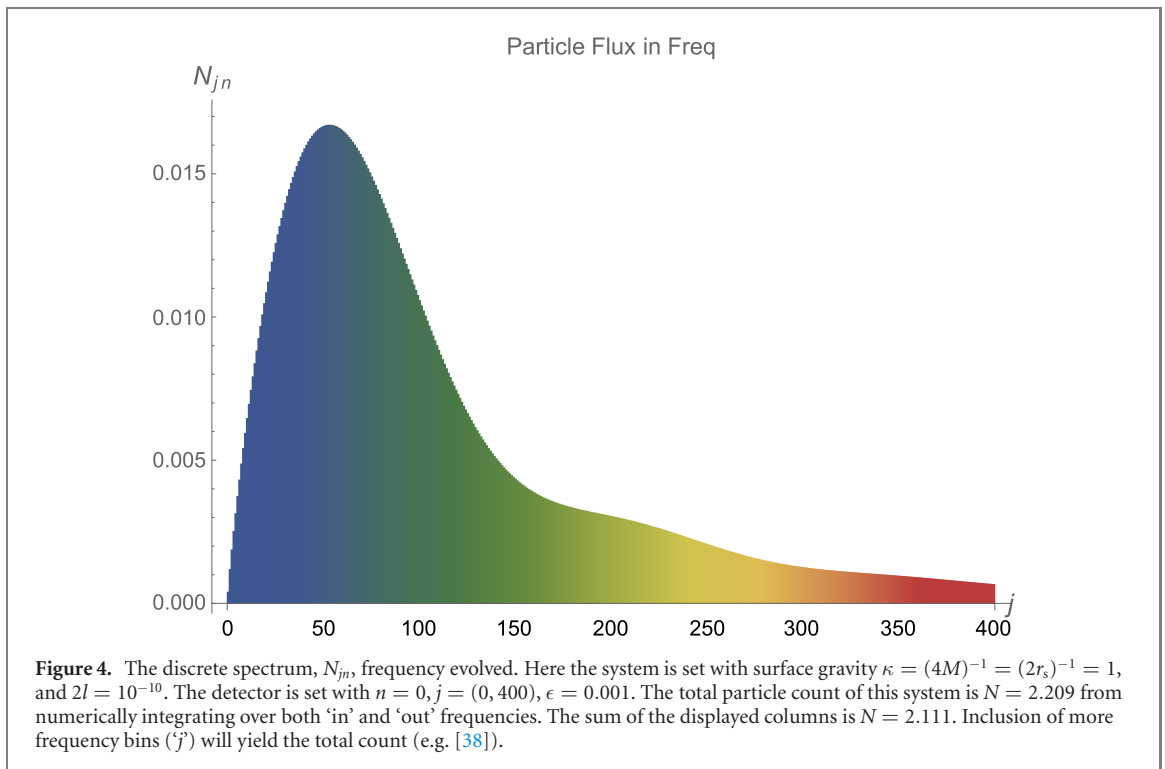
The exact total energy expression is in appendix C, equation (C10). Since the energy is finite, the evaporation process eventually stops. Geometrically, the classical Schwarzschild vacuum dictates $l \ll r_s$, but here we can energetically motivate that small scale in order that the radiated energy is substantial enough to exhaust the black hole. Going further, using the full expression equation (C10) one can see that as r_s approaches l , the full mass will be radiated if l is of order l_p . The black hole mass is carried away by the radiation (along with the information via a turn-over of the Page curve, e.g. [34]). At least in the conformal case, this represents an improvement to the canonical case, where the energy emitted is infinite. To understand whether a remnant is left over, finite energy emission is insufficient; a constant red-shift in the modes in the asymptotic future will signal its presence. In our case there is no remnant, and the evaporation is complete.

3.4. Particle spectrum

The beta coefficients are computed exactly in the s-wave sector with the effective potential ignored [19]. The particle spectrum is found to be, up to a constant:

$$N_\omega = \frac{1}{e^{\omega/T} - 1}, \quad (31)$$

in leading order $r_s \gg l$, where $T = (4\pi r_s)^{-1}$, demonstrating a quasi-thermal radiation field. The fact that the spectrum is not exactly thermal, due to non-leading order corrections, (but is analytically known) means the information is transported on the radiation.



The particular deviation from thermality also allows for a finite total amount of particle production, for a given l , which is readily calculated [31] for a known black hole mass M . Frequency evolution can be resolved with the use of wave packets [2, 35–37] confirming the total particle count done in [19, 31]. With sufficiently small $l \ll r_s$, and good frequency resolution (small ϵ) on the particle detector, one can see the spectrum shape well-resolved in figure 4.

3.5. Temperature correction via surface gravity

The temperature is not exactly the classical horizon temperature. We want the limiting temperature outside the black hole, $r > r_s$. Computing via the usual expression for surface gravity of a static metric, $2\kappa = g'_{tt}(r)|_{r \rightarrow r_s}$, and $\kappa = 2\pi T$, we have

$$T = \frac{\Delta r_s}{4\pi \sqrt{\Delta^2 + l^2} (r_s + \sqrt{\Delta^2 + l^2})^2}. \quad (32)$$

For $l = 0$, in the limit $r \rightarrow r_s$ (from above), the temperature is $T_H = (4\pi r_s)^{-1}$. In general the temperature is maximum right outside the Schwarzschild radius and can be found with an exact expression. The corrected temperature to leading order is

$$\frac{T}{T_H} = 1 - 3 \left(\frac{l^2}{2r_s^2} \right)^{1/3}, \quad (33)$$

cooler but generally a negligible decrease in temperature.

3.6. Limitations of the model

It is worthwhile to comment on a few potential extensions of this work and current limitations of the proposed toy model. In particular,

- One expects a non-static situation, with increasing temperature associated with the decreasing black hole mass during evaporation. This is not modeled. However, it does not appear that this is intractable, e.g. via introduction of suitably creative matching conditions.
- There is non-trivial spatial curvature in the region just outside the black hole, $\Delta \equiv (r - r_s) \sim l$, i.e. within a few Planck lengths of the horizon. This regime requires a full theory of quantum gravity and is beyond the scope of the current work.
- Conformal asymmetry calculation for the stress tensor in $3 + 1$ dimensions and total energy production has not been attempted. Besides issues of vacuum polarization, it is well known that conformal symmetry greatly simplifies the form of the stress tensor.

- While the mode solutions are good approximations where $R \approx 0$, away from the horizon, they will not satisfy the corresponding wave equation if conformal coupling is chosen, $\xi = 1/6$, because $R \neq 0$ near the horizon. For minimal coupling, $\xi = 0$, the equation of motion is simple and the modes studied here are appropriate but the theory will not be conformally invariant in $3 + 1$ dimensions in the massless limit.

Despite these extensions, the metric as is, equation (12), is a conceptually transparent geometry for modeling some aspects of unitary black hole radiance. The strength of this approach is the use of the preservation of unitarity (elaborated on in the next section) as a guiding principle with which to push the conventional model on the gravity side. Rather than taking the matching condition as being dynamically determined by the matter, the matching condition is treated as a given. While this may be considered a weakness, in the light of quantum pure evolution this approach appears as an additional strength accompanying the usual and simple quantum mechanical system of the moving mirror model.

The second bullet point highlights the new metric assertion that the horizon, as observed by outside observers, is ‘special’ in a certain sense. That is, from the point of view of an outside observer, the length scale modification near the horizon results in a boundary-type surface, seemingly possessing microphysical degrees of freedom that will appear in the quantum Hamiltonian used to describe the observable system. These degrees of freedom are sufficiently complex that they behave ergodically and lead to a coarse-grained dissipative description of the horizon with quasi-thermal radiation for most of the lifetime. This character of the horizon is most simply seen by the globally relevant metric equation (A23), a stationary non-collapse state solution of the star. However, despite this specialness, we consider these results in harmony with the complementarity (argued by [39]) between appraisals made by freely falling observers who cross the event horizon and those made by distant observers. Our results speak less to free-fall observations and more to outside measurements. This notion is supported by the consistency of the total energy carried by the particles and the total energy from the stress tensor (mirror analog), which are in agreement [19, 31], and measured only by distant observers.

As we have emphasized, we consider unitarity inviolable (e.g. Postulate 1 of [39]). Adopting this physical principle *a priori* resulted in the modified metric. The new metric with quantum length scale has strong curvature near the event horizon and is a clear invariant signal of its presence. In the sense that the equivalence principle is the basis for the belief that a freely falling observer experiences nothing out of the ordinary when crossing the event horizon of a very massive black hole, our model suggests otherwise. We consider these results as a thermodynamic addendum to the equivalence principle, in the same sense that the Unruh effect [3] is not considered a violation of the equivalence principle but a complement to it.

3.7. Unitary measure

To characterize quantum purity one can take the key dynamical behavior of the mirror—asymptotic inertia, which is responsible for information preservation—and define a ‘topological rapidity’, if you will, borrowing the notion that tearing is not allowed, only stretching. This rapidity, η , can be used in the curved spacetime context to consider the asymptotic inertial geometric counterpart of the mirror’s rapidity $\eta = \tanh^{-1}\beta$, where β is the velocity in units of the speed of light.

Helpful inspiration comes from the behavior of the quantum modes via the longitudinal relativistic Doppler factor:

$$D \equiv e^\eta = \sqrt{\frac{1+\beta}{1-\beta}}, \quad (34)$$

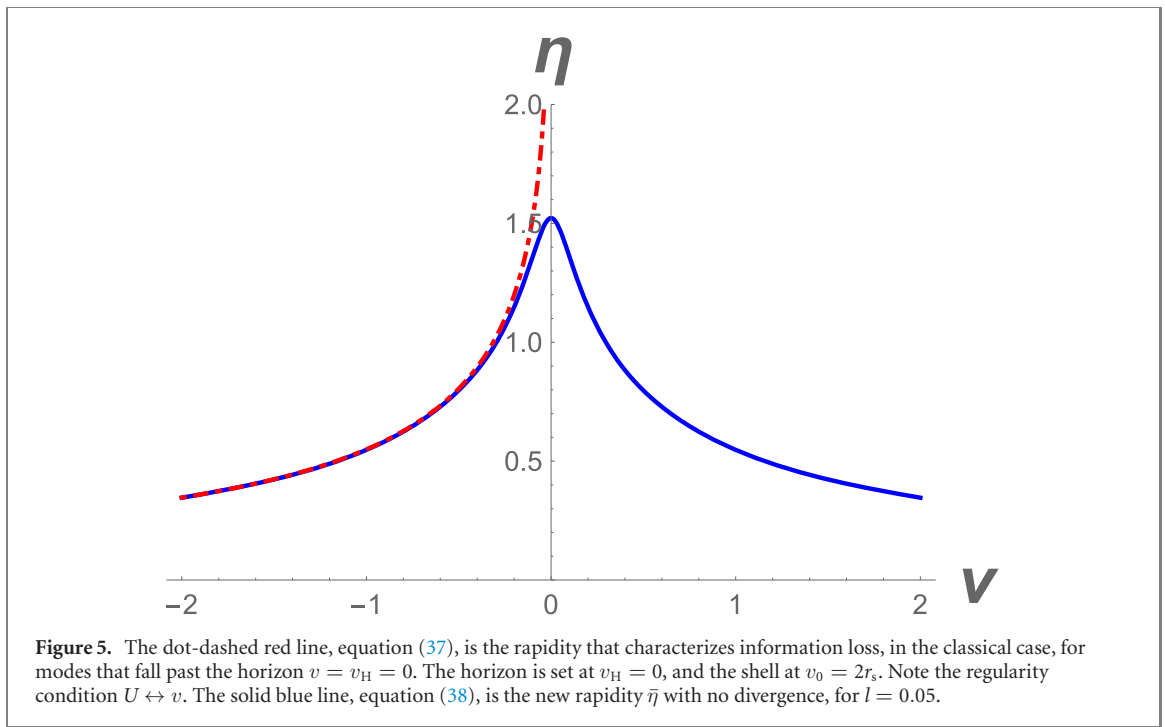
which has a divergence if the emitting source is moving at the speed of light, $\beta = 1$ (or zero if $\beta = -1$). In null coordinates, we see

$$\frac{dv}{du} = \frac{d(t+x)}{d(t-x)} = \frac{1+\beta}{1-\beta} = e^{2\eta} = D^2. \quad (35)$$

In our geometric context, between inside and outside coordinates, we can define in analogy to equation (35), via regularity $U \leftrightarrow v$, a rapidity of the worldline of the origin, $u(U)$,

$$|\eta| = \frac{1}{2} \ln \frac{du(U)}{dU}. \quad (36)$$

Information loss can be thought of as a divergence in this rapidity for some time U . Worldlines, after all, are considered time-like, $\eta \neq \infty$.



In the black mirror-black hole case,

$$|\eta| = \frac{1}{2} \ln \left(1 - \frac{2r_s}{U} \right), \quad (37)$$

one has a divergence for the time $U \rightarrow 0^-$. The inside time ends at the shell. Here the horizon is set at $v_H = 0$, and $v_0 = 2r_s$. The modes are lost in between $U = [0, 2r_s]$, corresponding to where the black hole singularity is located, absorbing the field: destroying it. This is the same as saying all modes that fall in past $v_H = 0$ get trapped in the black hole singularity. This information loss is characterized by an imaginary value of rapidity (for cases with light-like travel see e.g. [40–42]).

In the new geometry considered here, the rapidity of the origin,

$$|\bar{\eta}| \equiv \frac{1}{2} \ln \left(1 + \frac{2r_s}{\sqrt{U^2 + (2l)^2}} \right), \quad (38)$$

has no divergence for all real times U . In this chosen definition, we use the derivative taken with sign of U as negative. This sign will be fixed even when U is positive, avoiding the divergence at $U = [0, 2r_s]$; keeping the rapidity positive for $-\infty < U < +\infty$. The previous divergence at $U \rightarrow 0$ (or $v \rightarrow v_H = 0$) is cured such that

$$|\bar{\eta}|_{U \rightarrow 0} = \frac{1}{2} \ln \left(1 + \frac{r_s}{l} \right). \quad (39)$$

A finite maximum topological rapidity, i.e. quantum purity in this context, prevents the divergence. The classical and new rapidities are plotted in figure 5.

It is worth noting that rapidity and entanglement entropy [22] have a close relationship in the conformally symmetric context, $\eta = -6S$, demonstrating that a divergence in entanglement entropy also signals information loss.

4. Conclusion

We extend the classical black hole with a toy model that preserves unitarity, demonstrating consistence with quantum mechanics, in quasi-thermal particle production from the semi-classical black hole background vacuum, to first order in the Planck length, i.e. corrections are higher order $\mathcal{O}(l^2)$. The black hole description tightens the analogy to the physics of an accelerated boundary (moving mirror). This provides insights into how the equivalence principle applies from the emission of particles in quantum theory [43] to the geometric context of gravitation.

The curved spacetime solution possesses several desired characteristics not present in previously known solutions, in particular giving

- Construction of a geometry that reduces to the classical Schwarzschild metric but extends it with by incorporating another length scale, much smaller than the Schwarzschild radius, connected with the Planck length. This ‘quantum’ Schwarzschild metric, equation (12), is capable of describing the evolution of a pure state that remains unitary.
- Demonstration that quasi-thermal equilibrium energy flux existing in the 1 + 1 conformally symmetric case hints that the 3 + 1 stress tensor may exhibit similar behavior consistent with the Planck distribution of the particle spectrum from the s -wave sector.
- Demonstration of finite energy in the 1 + 1 conformally symmetric case, implying that the radiation process stops, signaling an end to evaporation.
- Introduction of a modified matching condition, and a quantum Regge–Wheeler coordinate sufficiently describing field modes for a collapse to black hole model. The limits for the classical model are approached for $\mathcal{R} \equiv l/r_s \rightarrow 0$.

Due to natural, quantum pure plane wave form modes in the early past and late future, it is clear no information is lost. We connect this to complete evaporation of the black hole, demonstrating the relevant coordinate transformations. The lack of soft particle divergence, the finite energy and particle count, and the lack of a remnant further point to this solution as an interesting and potentially fruitful laboratory for exploration of quantum particle production in the Universe.

Acknowledgments

Funding from state-targeted program ‘Center of Excellence for Fundamental and Applied Physics’ (BR05236454) by the Ministry of Education and Science of the Republic of Kazakhstan is acknowledged. MG is funded by the ORAU FY2018-SGP-1-STMM Faculty Development Competitive Research Grant No. 090118FD5350 at Nazarbayev University. EL is supported in part by the Energetic Cosmos Laboratory and by the US Department of Energy, Office of Science, Office of High Energy Physics, under Award DE-SC-0007867 and Contract No. DE-AC02-05CH11231.

Data availability statement

All data that support the findings of this study are included within the article (and any supplementary files).

Appendix A. Spacetime quantities

Here we present in detail many of the geometric objects of the metric equation (12). We write $z \equiv +\sqrt{\Delta^2 + l^2}$.

A.1. Connections

The Christoffel symbols are symmetric under interchange of the last two indices, so only the independent components are displayed. The indices 1, 2, 3, 4 represent t, r, θ, ϕ . The results are

$$\Gamma_{21}^1 = \frac{\Delta r_s}{2z^2(z+r_s)} \rightarrow \frac{r_s}{2r\Delta} \left[1 + \mathcal{O}\left(\frac{l^2}{\Delta^2}\right) + \mathcal{O}\left(\frac{l^2}{r\Delta}\right) \right] \quad (\text{A1})$$

$$\Gamma_{11}^2 = \frac{\Delta r_s}{2(z+r_s)^3} \rightarrow \frac{r_s \Delta}{2r^3} \left[1 + \mathcal{O}\left(\frac{l^2}{r\Delta}\right) \right] \quad (\text{A2})$$

$$\Gamma_{22}^2 = -\frac{\Delta r_s}{2z^2(z+r_s)} \rightarrow -\frac{r_s}{2r\Delta} \left[1 + \mathcal{O}\left(\frac{l^2}{\Delta^2}\right) + \mathcal{O}\left(\frac{l^2}{r\Delta}\right) \right] \quad (\text{A3})$$

$$\Gamma_{33}^2 = -\frac{zr}{z+r_s} \rightarrow -\Delta \left[1 + \mathcal{O}\left(\frac{l^2}{\Delta^2}\right) + \mathcal{O}\left(\frac{l^2}{r\Delta}\right) \right] \quad (\text{A4})$$

$$\Gamma_{44}^2 = -\frac{zr}{z+r_s} \sin^2 \theta \rightarrow -\Delta \sin^2 \theta \left[1 + \mathcal{O}\left(\frac{l^2}{\Delta^2}\right) + \mathcal{O}\left(\frac{l^2}{r\Delta}\right) \right], \quad (\text{A5})$$

where the right arrow gives the lowest order correction in l/Δ and l/r_s , with the classical limit being $l = 0$. The last four independent cases remain the usual classical Schwarzschild connections:

$$\Gamma_{32}^3 = \frac{1}{r}, \quad \Gamma_{44}^3 = -\cos \theta \sin \theta, \quad \Gamma_{42}^4 = \frac{1}{r}, \quad \Gamma_{43}^4 = \cot \theta. \quad (\text{A6})$$

A.2. Riemann tensor

The nonzero components are displayed by the following expressions. Here we use $R_{\mu\nu\sigma}^\lambda$ format. One can obtain, for example, R_{231}^1 from the R_{213}^1 using the antisymmetry of the Riemann tensor under exchange of the last two indices. The antisymmetry under exchange of the first two indices of $R_{\lambda\mu\nu\sigma}$ is not evident here because the components of $R_{\mu\nu\sigma}^\lambda$ are displayed.

$$R_{221}^1 = \frac{r_s(-2\Delta^4 + l^4 - \Delta^2 l^2 + l^2 z r_s)}{2z^5(z+r_s)^2}, \quad R_{331}^1 = \frac{\Delta r_s(\Delta+r_s)}{2z(z+r_s)^2}, \quad R_{441}^1 = \frac{\Delta r_s(\Delta+r_s)}{2z(z+r_s)^2} \sin^2 \theta \quad (\text{A7})$$

$$R_{121}^2 = \frac{r_s(-2\Delta^4 + l^4 - \Delta^2 l^2 + l^2 z r_s)}{2z^3(z+r_s)^4}, \quad R_{332}^2 = \frac{\Delta r_s(\Delta+r_s)}{2z(z+r_s)^2}, \quad R_{442}^2 = \frac{\Delta r_s(\Delta+r_s)}{2z(z+r_s)^2} \sin^2 \theta \quad (\text{A8})$$

$$R_{131}^3 = \frac{\Delta r_s}{2(\Delta+r_s)(z+r_s)^3}, \quad R_{232}^3 = -\frac{\Delta r_s}{2z^2(\Delta+r_s)(z+r_s)}, \quad R_{443}^3 = -\frac{r_s}{z+r_s} \sin^2 \theta \quad (\text{A9})$$

$$R_{141}^4 = \frac{\Delta r_s}{2(\Delta+r_s)(z+r_s)^3}, \quad R_{242}^4 = -\frac{\Delta r_s}{2z^2(\Delta+r_s)(z+r_s)}, \quad R_{343}^4 = \frac{r_s}{z+r_s} \quad (\text{A10})$$

A.3. Ricci tensor

$$R_{11} = \frac{r_s \left(l^2 (r_s - 3z) + \frac{2z^2(\sqrt{z^2-l^2+z}r_s)}{\sqrt{z^2-l^2+r_s}} \right)}{2z^2(r_s-z)^4}, \quad R_{22} = \frac{-r_s \left(l^2 (r_s - 3z) + \frac{2z^2(\sqrt{z^2-l^2+z}r_s)}{\sqrt{z^2-l^2+r_s}} \right)}{2z^4(r_s-z)^2}. \quad (\text{A11})$$

$$R_{33} = \frac{r_s \left((\sqrt{z^2-l^2+z}r_s - l^2) \right)}{z(r_s-z)^2}, \quad R_{44} = \frac{r_s \left((\sqrt{z^2-l^2+z}r_s - l^2) \right)}{z(r_s-z)^2} \sin^2 \theta. \quad (\text{A12})$$

A.4. Einstein tensor

$$G_{11} = \frac{r_s(z-\Delta)(r+z)}{r^2(r_s+z)^3}, \quad G_{22} = -\frac{r_s(z-\Delta)(r+z)}{z^2 r^2 (r_s+z)}. \quad (\text{A13})$$

$$G_{33} = \frac{r_s(z-\Delta)r \left(r_s(\Delta^2 + r_s(\Delta+z) + z^2 + 4\Delta z) + 3\Delta z(\Delta+z) \right)}{2z^3(r_s+z)^3}. \quad (\text{A14})$$

$$G_{44} = \frac{r_s(z-\Delta)r \left(r_s(\Delta^2 + r_s(\Delta+z) + z^2 + 4\Delta z) + 3\Delta z(\Delta+z) \right)}{2z^3(r_s+z)^3} \sin^2 \theta. \quad (\text{A15})$$

A.5. Ricci scalar

$$R = \frac{r_s(z-\Delta) \left(r_s \left(r_s(-2\Delta^2 - r_s(\Delta+z) + z^2 - 5\Delta z) + (\Delta+z)(-\Delta^2 + 4z^2 - 6\Delta z) \right) + z(\Delta+z)(2z^2 - 3\Delta^2) \right)}{z^3 r^2 (r_s+z)^3} \quad (\text{A16})$$

At leading order in l/Δ and l/r_s ,

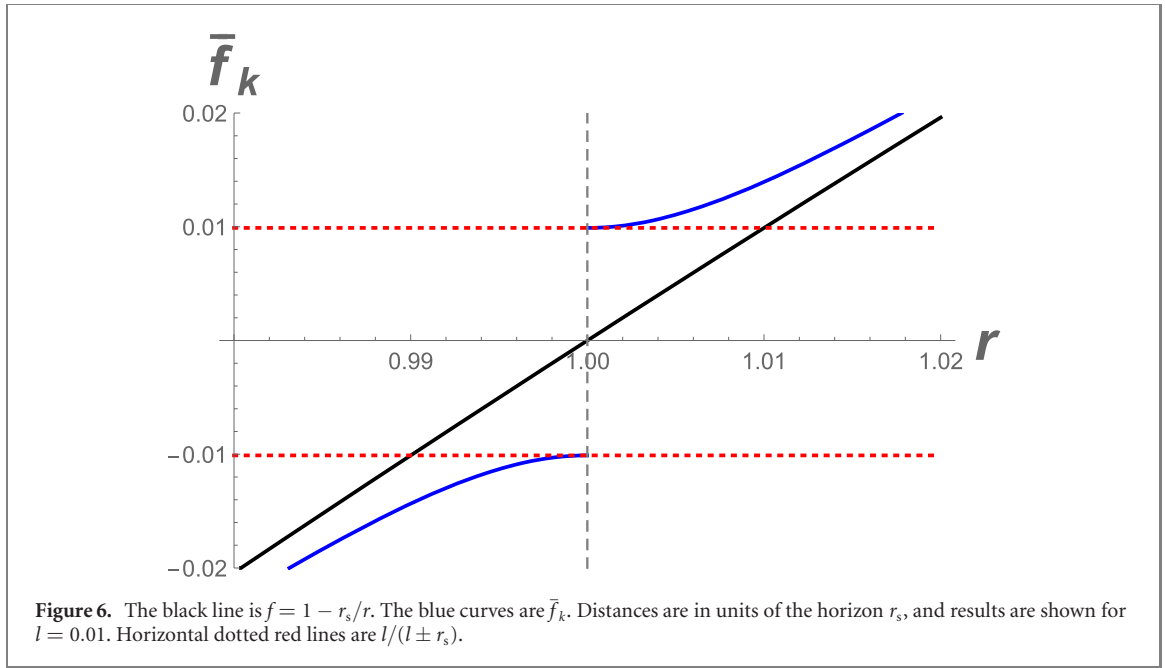
$$R = 0 - \frac{r_s l^2}{r^5} \left(1 + \frac{r_s}{\Delta} \right)^3. \quad (\text{A17})$$

Note that outside the black hole the Ricci scalar does not vanish, as in the classical case, reflecting the particle production. If the nonzero Ricci scalar is due to a particle flux, one might expect it to behave at large distances as $1/r^2$, but instead we have $1/r^2 \times (r_{sc}/r)^3$ where $r_{sc} = \sqrt[3]{r_s l^2}$. This is vaguely reminiscent of braneworld gravity where a screening scale of the higher dimension effects occurs for $r_{sc} = \sqrt[3]{r_s r_c^2}$, where r_c is the crossover scale related to the higher dimensional Planck length.

Within experimental bounds, (e.g. event horizon telescope or gravitational wave observations, see [44] and references therein for horizon scale modifications of the classical geometry of a black hole) the quantum Schwarzschild metric has the potential to be more consistent with quantum theory than its classical counterpart because unitarity is preserved in the gravitational collapse geometry. By relaxing the strict definition of the classical $R=0$ vacuum of general relativity near the black hole horizon, information loss can be avoided.

A.6. Kretschmann scalar

$$K = \frac{r_s^2 \left(4z^8 (r_s+z)^4 + 4\Delta^2 z^6 r^2 (r_s+z)^2 + z^2 r^4 (r_s(z-\Delta)(\Delta+z) + z^3 - 3\Delta^2 z)^2 \right)}{z^8 r^4 (r_s+z)^6} \quad (\text{A18})$$



A.7. Limits: $r \rightarrow \infty$, $r \rightarrow r_s$, or $l \rightarrow 0$

$$\lim_{r \rightarrow \infty} R = 0, \quad \lim_{r \rightarrow r_s} R = \frac{2l^2 + 2lr_s - r_s^2}{lr_s(l + r_s)^2}, \quad \lim_{l \rightarrow 0} R = 0. \quad (\text{A19})$$

$$\lim_{r \rightarrow \infty} K = 0, \quad \lim_{r \rightarrow r_s} K = \frac{4l^4 + 8l^3 r_s + 4l^2 r_s^2 + r_s^4}{l^2 r_s^2 (l + r_s)^4}, \quad \lim_{l \rightarrow 0} K = \frac{12r_s^2}{r^6}. \quad (\text{A20})$$

A.8. Leading order at $r \rightarrow \infty$

$$R = -\frac{l^2 r_s}{r^5} + \mathcal{O}(r^{-6}). \quad (\text{A21})$$

$$K = \frac{12r_s^2}{r^6} - \frac{40l^2 r_s^2}{r^8} + \mathcal{O}(r^{-9}). \quad (\text{A22})$$

A.9. A global non-collapse geometry

$$ds^2 = -\bar{f}_k dt^2 + \bar{f}_k^{-1} dr^2 + r^2 d\Omega, \quad (\text{A23})$$

Here

$$\frac{d\bar{r}^*}{dr} = \bar{f}_k^{-1} = 1 + k \frac{r_s}{z}, \quad (\text{A24})$$

where $k = -1, 0, +1$, for inside, on, and outside the Schwarzschild radius, i.e. $k = \text{sign}(\Delta)$. Figure 6 plots $\bar{f}_k(r)$. Note the removable discontinuity at the horizon.

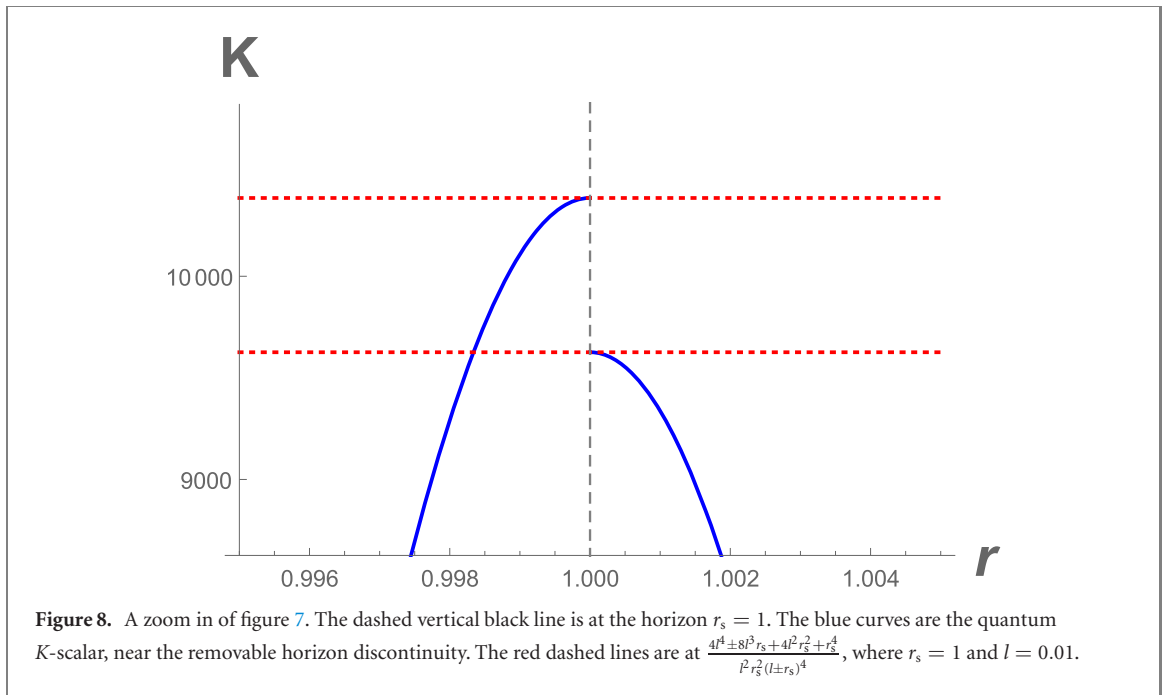
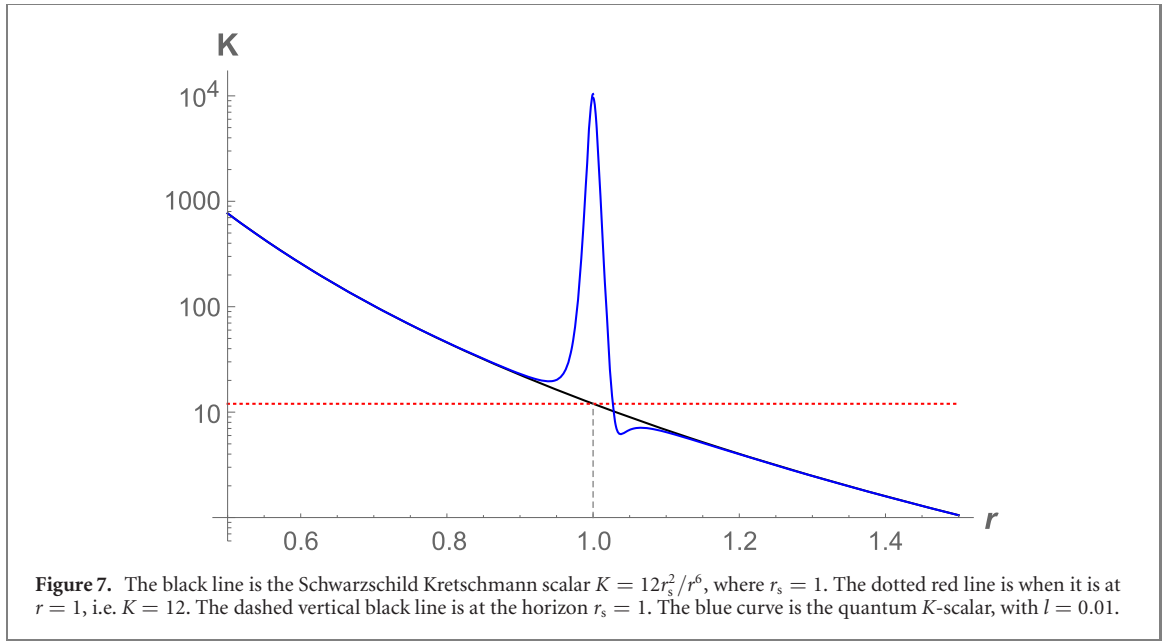
Figure 7 shows the Kretschmann scalar, in the quantum and classical versions. Again, there is modification near the horizon, and a small discontinuity at the horizon, proportional to l —best seen in the zoomed version figure 8.

The Ricci scalar is exhibited in figure 9, again showing modification near the horizon. Here the discontinuity is proportional to $1/l$.

Appendix B. Inside coordinate collapse geometry

The canonical case of a collapsing shell of matter described both inside and outside will utilize the geometry of equation (12) and is expressed in null ‘inside’ coordinates to give a complete cover of the spacetime, (see e.g. [12] for detail on outside coordinate representation),

$$ds^2 = \begin{cases} -dU dV, & \text{for } v \leq v_0, \\ -\bar{f}(u, v) \bar{f}^{-1}(u, v_0) dU dV, & \text{for } v \geq v_0. \end{cases} \quad (\text{B1})$$



where U and V are the inside coordinates, as mentioned before,

$$U = T - r, \quad V = T + r, \tag{B2}$$

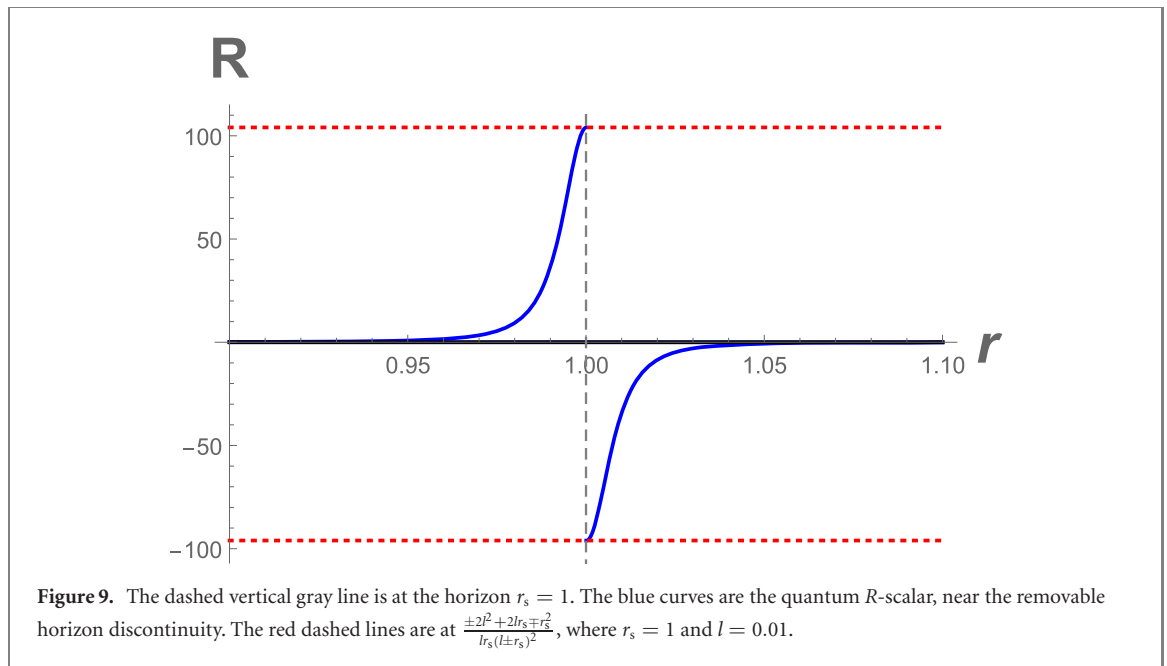
and the new tortoise coordinate, equation (10), helps us define u and v as the outside coordinates dropping the bar notation, as also previously given,

$$u = t - r^*, \quad v = t + r^*. \tag{B3}$$

For clarity, and without loss of generality in 3 + 1 dimensions, we have dropped the $r^2 d\Omega$ pieces of the metric on the two-sphere. The shell or shock wave is located at v_0 , where the horizon $v_H \equiv v_0 - 2r_s$, is set to $v_H = 0$ for simplicity, so that $v_0 = 2r_s$. The metric is sewn on the shell v_0 , from inside to outside:

$$\lim_{v_0 \rightarrow 2r_s} \bar{f}(u, v) \bar{f}^{-1}(u, v_0) = 1. \tag{B4}$$

The metric is also regular, like the canonical case, at the horizon $r = r_s$, but instead of $f = 0$, we have $\bar{f} = l/(l + r_s) \approx l/r_s$.



Appendix C. 1 + 1, energy flux, total energy

C.1. From 1 + 1 black mirror to 1 + 1 black hole

In the quantum pure black mirror [19], the calculations are most efficiently done using time as a function of space, $t(x)$,

$$t(x) = -x - 2l \sinh \frac{x}{r_s}, \quad (\text{C1})$$

where we have anticipated the black hole collapse model by converting the parameters to the appropriate black hole quantities. In 1 + 1 dimensions, the single dimension of space, x , must be generalized to be more closely recognized in the radial black hole case, which can be done by inspection of its range, $+\infty$ to $-\infty$. The matching condition,

$$u(U) = U - 2r_s \sinh^{-1} \left| \frac{U}{2l} \right|, \quad (\text{C2})$$

is re-arranged to give

$$|U| = 2l \sinh \left(\frac{U - u}{2r_s} \right), \quad (\text{C3})$$

where we are now free to choose the negative sign because U starts off negative at the beginning of collapse:

$$U = -2l \sinh \left(\frac{U - u}{2r_s} \right). \quad (\text{C4})$$

Using regularity, $U \leftrightarrow v$, it's clear that to describe the field modes our expression becomes in the outside null coordinates,

$$v = -2l \sinh \left(\frac{v - u}{2r_s} \right), \quad (\text{C5})$$

and in terms of space-time coordinates, we see

$$t(r^*) = -r^* - 2l \sinh \left(\frac{r^*}{r_s} \right). \quad (\text{C6})$$

Therefore, in going from the 1 + 1 dimensions of the mirror model to the 1 + 1 dimensions of the spherically symmetric black hole collapse model, one replaces the spatial coordinate x with the tortoise coordinate: $x \leftrightarrow r^*$.

C.2. Energy flux with NEF and plateau; 1 + 1 case

Using the $t(r^*)$ function, and appropriately expressed coordinate transformed Schwarzsian, the energy flux can be expressed as a function of r^* ,

$$F(r^*) = \langle \text{in} | : T_{uu} : | \text{in} \rangle = \frac{r_s \left(4l \cosh\left(\frac{r^*}{r_s}\right) - 3 \operatorname{sech}\left(\frac{r^*}{r_s}\right) \left[2l + r_s \operatorname{sech}\left(\frac{r^*}{r_s}\right) \right] + r_s \right)}{192\pi \left[l \cosh\left(\frac{r^*}{r_s}\right) + r_s \right]^4}. \quad (\text{C7})$$

A plot of this function is given in figure 2 of [19], showing the thermal plateau and the negative energy flux spike.

C.3. Finite total energy; 1 + 1 case

The total energy is found by integrating the energy flux,

$$E = \int F du = \int_{+\infty}^{-\infty} F(r^*) \left(\frac{dt(r^*)}{dr^*} - 1 \right) dr^*, \quad (\text{C8})$$

over the Jacobian element, $du = dt - dr^*$, where the derivative is computed from equation (C6) as

$$\frac{dt(r^*)}{dr^*} = -1 - \frac{2l}{r_s} \cosh\left(\frac{r^*}{r_s}\right). \quad (\text{C9})$$

The result for the total finite energy emitted is

$$E = - \frac{2 \left(6l^4 - 9l^2 r_s^2 + 2r_s^4 \right) \tanh^{-1} \left(\frac{l-r_s}{\sqrt{r_s^2 - l^2}} \right) + \sqrt{r_s^2 - l^2} \left(3\pi l^3 - 6l^2 r_s - 3\pi l r_s^2 + 5r_s^3 \right)}{96\pi r_s^2 \left(r_s^2 - l^2 \right)^{3/2}}. \quad (\text{C10})$$

This result strengthens the physical consistency of the model in general (because it agrees with the Bogolubov coefficients) and specifically with the notion that the radiation must be limited in space and time.

ORCID iDs

Michael R R Good  <https://orcid.org/0000-0002-0460-1941>

Eric V Linder  <https://orcid.org/0000-0001-5536-9241>

References

- [1] Parker L 1968 *Phys. Rev. Lett.* **21** 562
- [2] Hawking S W 1975 *Commun. Math. Phys.* **43** 199
- [3] Unruh W G 1976 *Phys. Rev. D* **14** 870
- [4] DeWitt B S 1975 *Phys. Rep.* **19** 295
- [5] Fulling S A and Davies P C W 1976 *Proc. R. Soc. A* **348** 393
- [6] Davies P C W and Fulling S A 1977 *Proc. R. Soc. A* **356** 237
- [7] Hawking S W, Perry M J and Strominger A 2016 *Phys. Rev. Lett.* **116** 231301
- [8] Chen P, Ong Y C and Yeom D-h. 2015 *Phys. Rep.* **603** 1
- [9] Hayden P and Preskill J 2007 *J. High Energy Phys.* **JHEP09(2007)120**
- [10] Parker L E and Toms D 2009 *Quantum Field Theory in Curved Spacetime* (Cambridge: Cambridge University Press)
- [11] Fabbri A and Navarro-Salas J 2005 *Modeling Black Hole Evaporation* (Singapore: World Scientific)
- [12] Wilczek F 1992 *Proceedings* (Houston: IAS Princeton)
- [13] Massar S and Parentani R 1996 *Phys. Rev. D* **54** 7444–58
- [14] Good M R R, Anderson P R and Evans C R 2016 *Phys. Rev. D* **94** 065010
- [15] Good M R R 2016 *2nd LeCoSPA Meeting*
- [16] Anderson P R, Good M R R and Evans C R 2015 *MG14*
- [17] Good M R R, Anderson P R and Evans C R 2016 *MG14*
- [18] Cong W, Tjoa E and Mann R B 2019 *J. High Energy Phys.* **JHEP06(2019)021**
- [19] Good M R R, Linder E V and Wilczek F 2020 *Phys. Rev. D* **101** 025012
- [20] Walker W R and Davies P C W 1982 *J. Phys. A: Math. Gen.* **15** L477
- [21] Good M R R and Linder E V 2019 *Phys. Rev. D* **99** 025009
- [22] Holzhey C, Larsen F and Wilczek F 1994 *Nucl. Phys. B* **424** 443
- [23] Chen P and Yeom D h 2017 *Phys. Rev. D* **96** 025016
- [24] Mukohyama S and Israel W 2000 *Phys. Rev. D* **62** 121501
- [25] Good M R R, Yelshibekov K and Ong Y C 2017 *J. High Energy Phys.* **JHEP03(2017)013**
- [26] Good M R R, Ong Y C, Myrzakul A and Yelshibekov K 2019 *Gen. Relativ. Grav.* **51** 92
- [27] Good M 2018 *Universe* **4** 122

- [28] Myrzakul A and Good M R R 2018 *MG15 Proc.*
- [29] Good M R R and Linder E V 2017 *Phys. Rev. D* **96** 125010
- [30] Birrell N D and Davies P C W 1982 *Quantum Fields in Curved Space* (Cambridge: Cambridge University Press)
- [31] Good M R R, Linder E V and Wilczek F 2020 *Mod. Phys. Lett. A* **35** 2040006
- [32] Hiscock W A 1981 *Phys. Rev. D* **23** 2813
- [33] Good M R R and Linder E V 2018 *Phys. Rev. D* **97** 065006
- [34] Hwang J, Park H, Yeom D-h. and Zoe H 2018 *J. Korean Phys. Soc.* **73** 1420
- [35] Good M R R, Anderson P R and Evans C R 2013 *Phys. Rev. D* **88** 025023
- [36] Good M R R 2017 *Kerson Huang Memorial* (Singapore: World Scientific)
- [37] Martin-Martinez E, Montero M and del Rey M 2013 *Phys. Rev. D* **87** 064038
- [38] Good M R R and Ong Y C 2015 *J. High Energy Phys. JHEP* **07** (2015) 145
- [39] Susskind L, Thorlacius L and Uglum J 1993 *Phys. Rev. D* **48** 3743–61
- [40] Carlitz R D and Willey R S 1987 *Phys. Rev. D* **36** 2327
- [41] Good M R R 2013 *Int. J. Mod. Phys. A* **28** 1350008
- [42] Hotta M, Schützhold R and Unruh W G 2015 *Phys. Rev. D* **91** 124060
- [43] Svidzinsky A A, Ben-Benjamin J S, Fulling S A and Page D N 2018 *Phys. Rev. Lett.* **121** 071301
- [44] Giddings S 2019 *Universe* **5** 201